Product Datasheet

Tyrosine Hydroxylase Antibody
NB300-109

Unit Size: 0.1 ml

Store at -20C. Avoid freeze-thaw cycles.

www.novusbio.com technical@novusbio.com

Reviews: 7 Publications: 219

Protocols, Publications, Related Products, Reviews, Research Tools and Images at:
www.novusbio.com/NB300-109

Updated 12/20/2023 v.20.1

NB300-109

Tyrosine Hydroxylase Antibody

Product Information	
Unit Size	0.1 ml
Concentration	Please see the vial label for concentration. If unlisted please contact technical services.
Storage	Store at -20C. Avoid freeze-thaw cycles.
Clonality	Polyclonal
Preservative	No Preservative
Isotype	IgG
Purity	Antigen Affinity-purified
Buffer	10 mM HEPES (pH 7.5), 0.15 M NaCl, 0.1 mg/mL BSA, 50% Glycerol
Target Molecular Weight	60 kDa

Product Description	
Host	Rabbit
Gene ID	7054
Gene Symbol	TH
Species	Human, Mouse, Rat, Chicken, Drosophila, Insect, Mammal
Reactivity Notes	Use in Chicken reported in scientific literature (PMID:34416224). Human reactivity reported in scientific literature (PMID:32756440). The tyrosine hydroxylase antibody recognizes all mammalian and at least some non-mammalian forms of the enzyme in Western blots and in IHC/IF. Insect reactivity reported in scientific literature (PMID: 27494326). .
Marker	Neuronal Marker
Specificity/Sensitivity	Specific for the ~60 kDa tyrosine hydroxylase protein.
Immunogen	SDS-denatured, native rat tyrosine hydroxylase purified from pheochromocytoma.

Product Application Details	
Applications	Western Blot, Simple Western, Immunocytochemistry/ Immunofluorescence, Immunohistochemistry, Immunohistochemistry-Frozen, Immunohistochemistry-Paraffin, Dual RNAscope ISH-IHC, Immunohistochemistry Free-Floating, Immunohistochemistry Whole-Mount, Knockout Validated
Recommended Dilutions	Western Blot 1:1000, Simple Western 2 ug/mL, Immunohistochemistry 1:10 - 1:500, Immunocytochemistry/ Immunofluorescence 1:1000, Immunohistochemistry-Paraffin 1:10 - 1:500, Immunohistochemistry-Frozen 1:1000, Immunohistochemistry Free-Floating, Immunohistochemistry Whole-Mount, Knockout Validated, Dual RNAscope ISH-IHC
Application Notes	Immunohistochemistry: use reported in literature (PMID: 22262884 and PMID: 23811324). Use in rat and mouse reported in customer review. Use in Immunohistochemistry Free floating reported in scientific literature (PMID 25731749). Use in Immunohistochemistry Whole mount reported in scientific literature (PMID: 26123524). Dual ISH-IHC validation (PMID: 29917232). In Simple Western only 10 - 15 uL of the recommended dilution is used per data point.

Images

Tyrosine hydroxylase immunoreactivity in the central complex and the lateral accessory lobe. A-D: Frontal sections (immunoperoxidase preparations, dorsal to the top). E: Horizontal section (immunofluorescent preparation, posterior to the top). Scale bars = 100 um. Image collected and cropped by CiteAb from the following publication (https://dx.plos.org/10.1371/journal.pone.0160531), licensed under a CC-BY license.	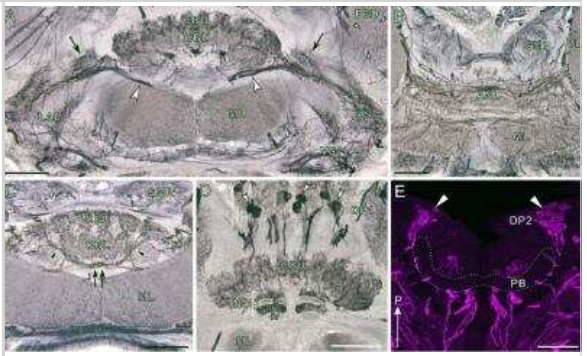
Dopamine neurons in the mouse substantia nigra. ICC/IF image submitted by a verified customer review.	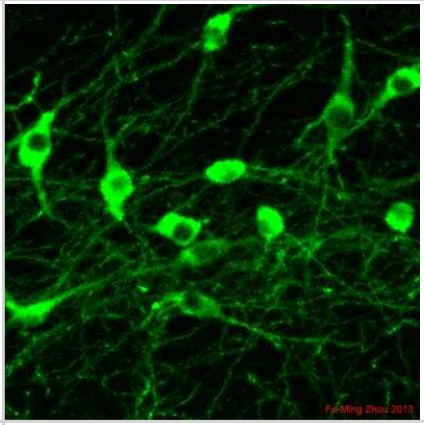
Simple Western lane view shows a specific band for Tyrosine Hydroxylase in 0.2 mg/mL of PC-12 lysate. This experiment was performed under reducing conditions using the 12-230 kDa separation system.	
Western blot of 10 ug of rat striatal lysate showing specific immunolabeling of the ~60 kDa tyrosine hydroxylase protein.	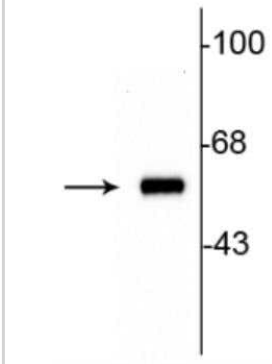

10x Magnification cryo-sections mouse: primary antibody: anti-rb TH: 1:500; o.n. secondary antibody: 1:500 dk-anti-rb DyLight488. IHC-Fr image submitted by a verified customer review.

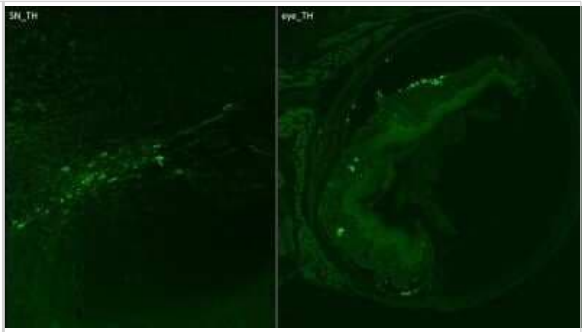

Tyrosine hydroxylase immunoreactivity in the mushroom body. All panels show a right brain hemisphere (dorsal to the top, medial to the right), except panels M-O (posterior to the top). Tyrosine hydroxylase (TH) immunoreactivity is shown in magenta (A, D, G, J, M) and synapsin immunoreactivity in green (B, E, H, K, N). Corresponding merged images in C, F, I, L, O. Scale bars = 100 um. Image collected and cropped by CiteAb from the following publication (https://dx.plos.org/10.1371/journal.pone.0160531), licensed under a CC-BY license.

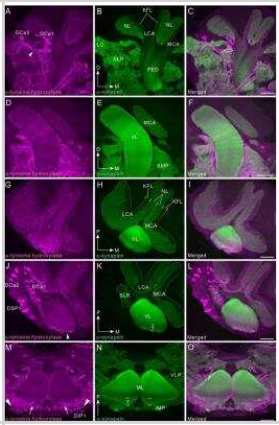

Western blot analysis confirms activation of UPR following Hotel protein lysates from the right adrenal medulla of saline (2RS) and RH groups (2RH) were subjected to Western blot analyses as described in methods. Proteins were separated by SDS-PAGE, electroblotted and the membranes were sequentially probed with antibodies specific to Grp78, Derlin1, TH and GAPDH. Similar results were obtained in two separate replicate experiments. Image collected and cropped by CiteAb from the following publication (https://dx.plos.org/10.1371/journal.pone.0172789), licensed under a CC-BY license.

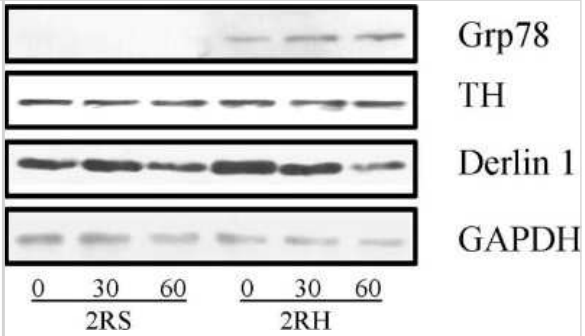

Impact of extrinsic and intrinsic hypoxia on catecholamine biosynthesis. Immunohistochemical staining showed an increased expression of Tyrosine Hydroxylase (red) in the necrotic and hypoxic core of the spheroid (DAPI, blue). Scale bar: 200 um. Image collected and cropped by CiteAb from the following publication (//pubmed.ncbi.nlm.nih.gov/31035382/) licensed under a CC-BY license.

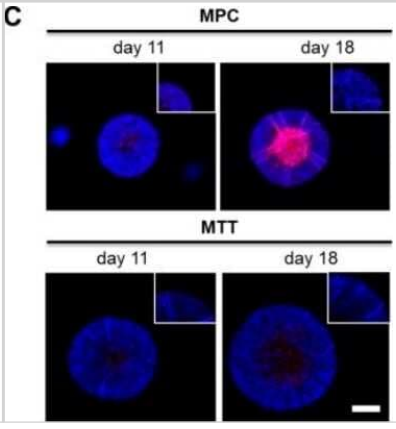

Immunohistochemical analysis of a formalin fixed and paraffin embedded rat brain tissue section using Tyrosine Hydroxylase antibody at 1:5000 dilution. The primary antibody binding to its antigen was detected using HRP anti-Polyvalent ready-to-use kit (Ultratek, 35368) with DAB (brown) and the sections were further counterstained using hematoxylin. Isotype control section was incubated with Rabbit IgG Isotype Control antibody and was processed under the same assay conditions. Tyrosine hydroxylase staining (brown) was observed in the test samples only and the signal was specifically localized to the neuronal cells.

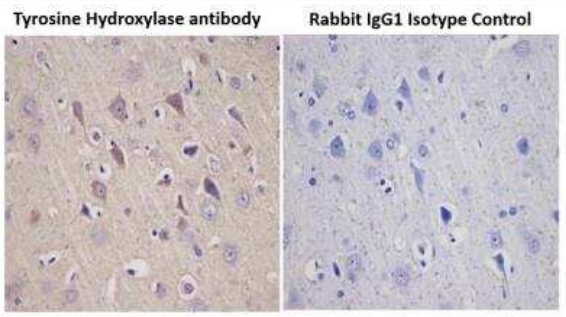

Immunostaining of whole-mount Drosophila brains using NB300-109 at 1:500 dilution. The tyrosine hydroxylase antibody worked really well and produced a bright staining with almost no background. Data courtesy of Dr. Olga Alekseenko, Neurobiology Dept. Harvard Medical School.

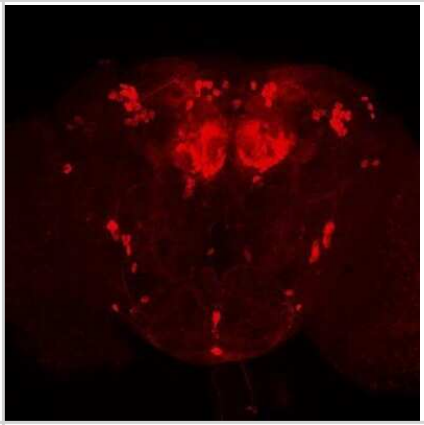

Immunohistochemical analysis of tyrosine hydroxylase in rat mesenteric artery-whole. ICC/IF image submitted by a verified customer review.

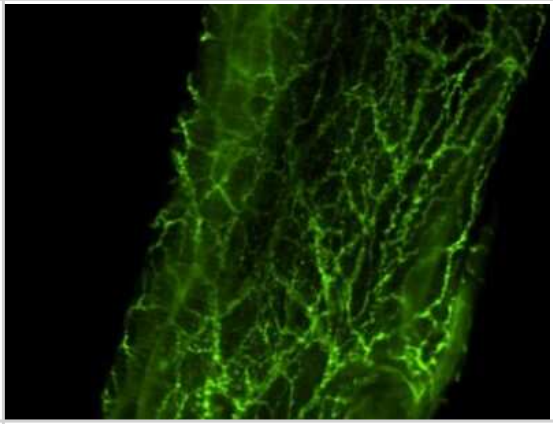

Western blot analysis confirms activation of UPR following RH.Total protein lysates from the right adrenal medulla of saline (2RS) and RH groups (2RH) were subjected to Western blot analyses as described in methods. Proteins were separated by SDS-PAGE, electroblotted and the membranes were sequentially probed with antibodies specific to Grp78, Derlin1, TH and GAPDH. Similar results were obtained in two separate replicate experiments.

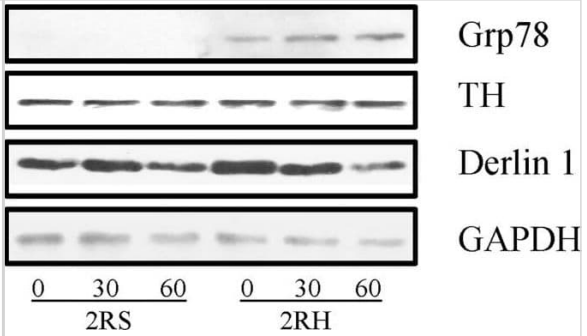

Image showing differentiation of neurospheres as evidenced morphologically (A) and through staining by Tyrosine Hydroxylase (B) to show the ability to derive dopaminergic neurons from the rat progenitor cells.

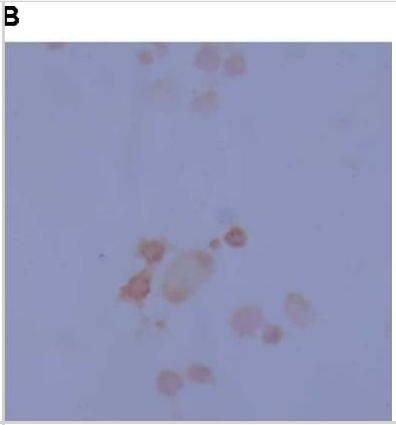

Validation of protein alterations and functional studies for pathways induced by genetic and toxic stress, and reversal of PD-related alterations following S-HSP90 inhibition. c) Western blot and quantification of rotenone stress increase in the p-TH:TH ratio and its reduction by PU-H71 (200 nM). p-ERK/ERK, cell viability control; beta-actin, protein loading control. Mean +/- SEM, n = 3 individual values from the different experiments shown as points, One-way ANOVA with Tukey's post-hoc, ***p < 0.001; **p < 0.01. d Total intracellular dopamine levels in PD mDA neurons in conditions of toxic stress and under PU-H71 rescue; Mean +/- SEM, n = 4-5 individual values from the different experiments shown as points, t-test, *p < 0.05. e PU-H71 treatment of rotenone- or CCCP-stressed mDA neurons significantly increases their viability, as measured by total ATP levels; means +/- SEM, n = 3-8 from independent differentiations, t-test, ***p < 0.001; **p < 0.01; *p < 0.05 Image collected and cropped by CiteAb from the following publication (https://pubmed.ncbi.nlm.nih.gov/30341316), licensed under a CC-BY licence.

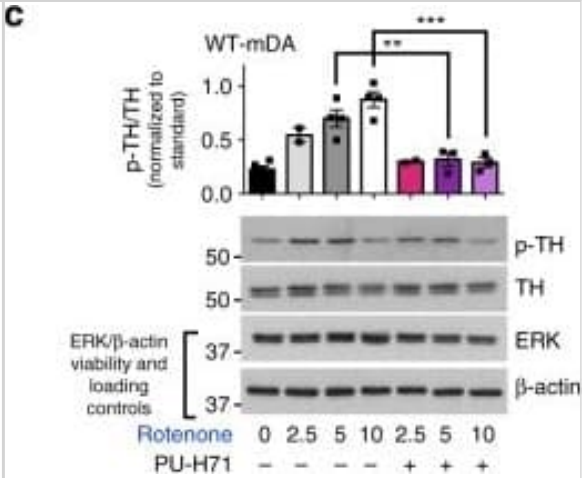

Characterization of the nigrostriatal pathway of LRRK2 conditional transgenic mice. A) Representative TH immunohistochemistry of the midbrain coronal sections of 22-month-old LRRK2 GS and GSDA transgenic and age-matched littermate controls. Image collected and cropped by CiteAb from the following publication (https://www.eneuro.org/lookup/doi/10.1523/ENEURO.0004-17.2017), licensed under a CC-BY licence.

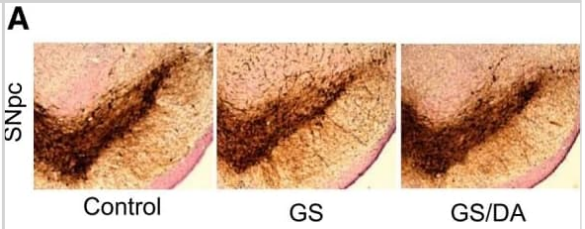

IHC-P analysis of hOGG1 protein expression in serous ovarian cancer: (A) Normal ovarian tissue treated with anti-hOGG1 antibody, biotinylated anti-rabbit IgG secondary antibody, and avidin-biotin-peroxidase complex, and counterstained with p-dimethylaminobenzaldehyde reagent (magnification 100 x); (B) serous cystadenoma with positive staining (magnification 200 x); (C) LG-SOC tissue with moderate positive staining (magnification 200 x); and (D) HG-SOC with negative staining (magnification 200 x). Black arrow pointed at the immunostained epithelial cells. Image collected and cropped by CiteAb from the following open publication (https://ovarianresearch.biomedcentral.com/articles/10.1186/1757-2215-6-74), licensed under a CC-BY license. Not internally tested by Novus Biologicals.

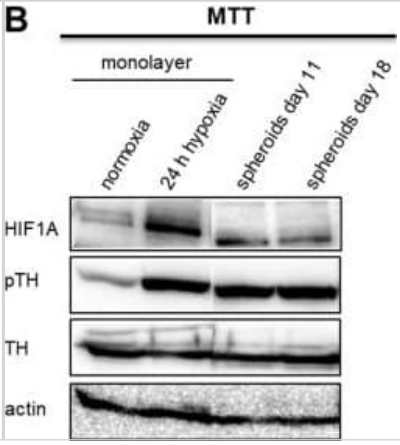

(a) Cell viability of MM cells exposed to increasing doses of LPS for 24 h. (b) Immunoblotting analysis of TLR4 protein expression levels in H929 and L363 cell lines after incubation with various LPS concentrations. Probing with β-ACTIN was used as total protein loading reference. (c) Flow cytometry analysis for TLR4 expression of MM cell lines before and after exposure to 1 µg/ml LPS for 24 h. (d) Cell viability of MM cell lines pre-treated with 0.5 µg/ml TLR4 inhibitor for 24 h before stimulation with LPS for 24 h. (e) Cell vViability of H929 and JJN3 cell lines exposed to increasing concentrations of TLR4 inhibitor for 48 h. β-ACTIN probing was used as reference for total protein input. Image collected and cropped by CiteAb from the following open publication (https://pubmed.ncbi.nlm.nih.gov/30824741), licensed under a CC-BY license. Not internally tested by Novus Biologicals.

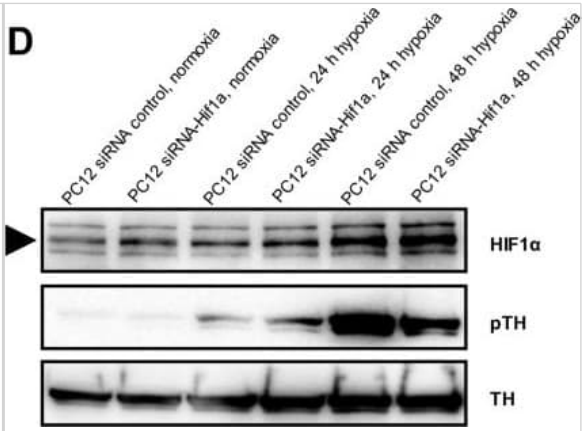

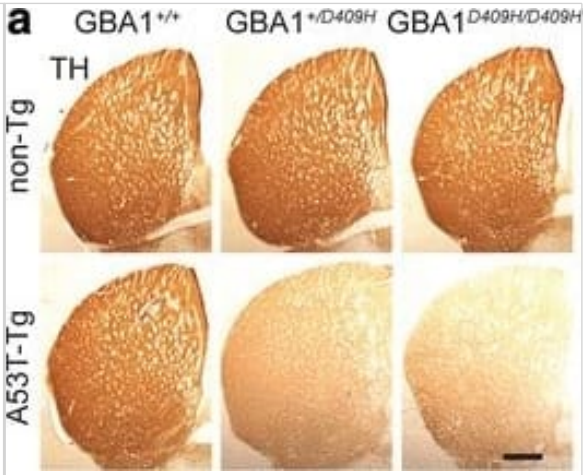

MI Exo enhance the ADMSC-mediated angiogenesis by promoting VEGF paracrine but not endothelial differentiation. (A) ADMSCs embedded in Matrigel were implanted subcutaneously on the back of mice, and MI models were then established. The implantation of cell-free Matrigel was served as negative control, and Matrigel plugs were removed on Day 14. (B) Representative macroscopic images and CD31 immunohistochemical staining of Matrigel plugs removed on Day 14. Scale bar, 5 mm (for macroscopic images); Scale bar, 100 μm (for immunohistochemical images); arrows indicate blood vessels. n = 4 mice per group. CD31 quantification is shown. Data are shown as mean ± SD. *, significantly different from the control group bearing with cell-free Matrigel; **, $p < 0.01$. #, significantly different from control group bearing with ADMSCs-embedded Matrigel; #, $p < 0.05$. (C) ADMSCs embedded in Matrigel were implanted subcutaneously on the back of mice. Con Exo and MI Exo (20 μg/each injection) were injected into the subcutaneous Matrigel plugs on Day 0, Day 5, and Day 10, respectively. PBS injection was served as the control. These Matrigel plugs were removed on Day 14. (D) Representative macroscopic images and CD31 immunohistochemical staining of Matrigel plugs removed on Day 14. Scale bar, 5 mm (for macroscopic images); Scale bar, 100 μm (for immunohistochemical images); arrows indicate blood vessels. n = 4 mice per group for the groups with cell-free Matrigel; n = 5 mice per group for the groups with ADMSCs-embedded Matrigel; CD31 quantification is shown. Data are shown as mean ± SD. *, significantly different from the control group bearing with cell-free Matrigel; **, $p < 0.01$. #, significantly different from control group bearing with ADMSCs-embedded Matrigel; #, $p < 0.05$. After being treated with Con Exo or MI Exo for 10 days following endothelial induction by EGM-2 medium, the protein and relative mRNA level for Cd31 and Vegf was assessed by confocal microscopy (E) and qRT-PCR (F), respectively. For E, cells were labelled with CD31 and VEGF (green), and nuclei were stained with DAPI (blue). Scale bar, 50 μm. Representative images of two independent experiments are shown. For F, data are shown as mean ± SD of four independent experiments for Cd31 and five independent experiments for Vegf. After being treated with Con Exo or MI Exo for 3 days, the level of secreted VEGF was detected by ELISA (G), and the expression of cellular VEGF was determined by western blotting (H). For G, two independent experiments were performed. Data are shown as mean ± SD. *, significantly different from control; **, $p < 0.01$. #, significantly different from Con Exo; #, $p < 0.05$. For H, representative images of three independent experiments are shown. Exosomal lysates of Con Exo and MI Exo were derived from an equal volume of serum. WCL, whole cell lysate derived from ADMSCs. (I) Tube formation analysis of ADMSCs after treatment with Con Exo and MI Exo for 5 h. Average tube length was quantified. Data are shown as mean ± SD from three independent experiments. *, significantly different from control; **, $p < 0.01$. #, significantly different from Con Exo; #, $p < 0.05$. One-way ANOVA followed by Tukey's post-test was performed (B, D, F, G and I). Image collected and cropped by CiteAb from the following open publication (https://pubmed.ncbi.nlm.nih.gov/31938051), licensed under a CC-BY license. Not internally tested by Novus Biologicals.

Abnormal Paneth cells show ER stress.(A, B) Representative transmission electron microscopy images of Paneth cells at the base of ileal crypts in (A) ICR and (B) SAMP1/YitFc mice. Scale bars indicate 2 μm. (C, D) Quantitative analysis of (C) granule number and (D) ER lumen diameter in Paneth cells (n = 3/each week for SAMP1/YitFc mice). For the measurements, three Paneth cells were randomly selected from each mouse. (E) SDS–PAGE Western blot analysis of ER stress markers, pIRE1α, ATF4, cleaved-ATF6, and GRP78 in ileal crypts (n = 4/each group). Total-IRE1α and HPRT1 was used as loading control. (F) Relative expression level of ER stress markers calculated from the band intensity. Error bars represent mean ± SEM. (C, D, F) Statistical significance was evaluated by t test in (C, D), and one-way ANOVA followed by Tukey's post hoc test in (F). P < 0.05 was considered statistically significant. *P < 0.05, †P < 0.01, §P < 0.001. E, ER; G, granules; N, nucleus; n.s., not significant. Image collected and cropped by CiteAb from the following open publication (https://pubmed.ncbi.nlm.nih.gov/32345659), licensed under a CC-BY license. Not internally tested by Novus Biologicals.

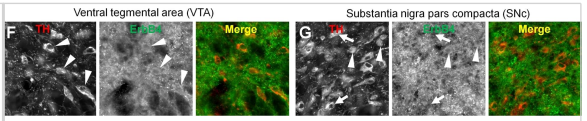

Dnmt3a1 decreases lipid droplet accumulation in the early stage of adipocyte differentiation. (A) Representative images of oil red O staining (red) and DAPI staining (blue) after transfection with pSDS-Dnmt3a1 and pSDS-NC for 48 h are showed; scale bar: 25 μm. (B) Lipid droplet content by oil red O staining and extraction method of cells transfected with pSDS-Dnmt3a1 and pSDS-NC for 48 h. Values represent mean ± SEM from three independent experiments. □□P < 0.01. (C) Representative images of oil red O staining (red) and DAPI staining (blue) after transfection with si-Dnmt3a1 and si-NC for 48 h are showed; scale bar: 25 μm. (D) Lipid droplet content by oil red O staining and the extraction method of cells transfected with si-Dnmt3a1 and si-NC for 48 h. Values represent mean ± SEM from three independent experiments. □P < 0.05. (E) Relative mRNA level of some general genes implicated in adipogenesis or energy homeostasis induced by pSDS-Dnmt3a1 and pSDS-NC into cells. Values represent mean ± SEM from four separate experiments. □P < 0.05, □□P < 0.01, and □□□P < 0.001. (F) Protein expression of some general adipose genes induced by pSDS-Dnmt3a1 and pSDS-NC into cells. (G) Relative mRNA level of some general genes involved in adipogenesis or energy homeostasis after transfection with si-Dnmt3a1 and si-NC into cells for 48 h. Values represent mean ± SEM from four separate experiments. □P < 0.05, □□P < 0.01, and □□□P < 0.001. (H) Protein expression of some general genes involved in adipogenesis at 48 h after transfection by si-Dnmt3a1 and si-NC into cells. The band intensity of Western blotting was obtained by averaging the data from three independent experiments. Image collected and cropped by CiteAb from the following open publication (https://pubmed.ncbi.nlm.nih.gov/30333755), licensed under a CC-BY license. Not internally tested by Novus Biologicals.

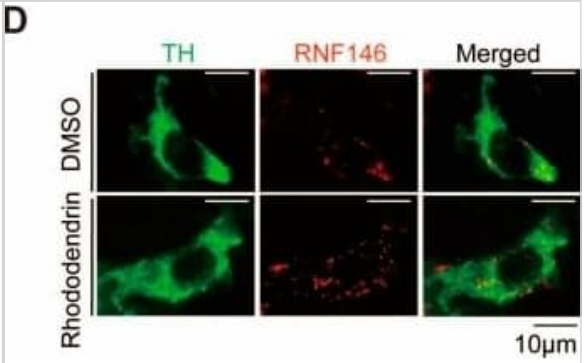

Localization of candidate RNAs at telomeres.Localization of SNORD17 (A) and NEAT1 (B) at telomeres in human U-2 OS cells. Cells were fixed and sequentially incubated with Abs against TRF-2 and AlexaFluor 488-conjugated anti-mouse IgG. Subsequently, the cells were hybridized with the RNA probes and subjected to fluorescence microscopy. Three different cells are shown. Image collected and cropped by CiteAb from the following open publication (https://pubmed.ncbi.nlm.nih.gov/25874893), licensed under a CC-BY license. Not internally tested by Novus Biologicals.

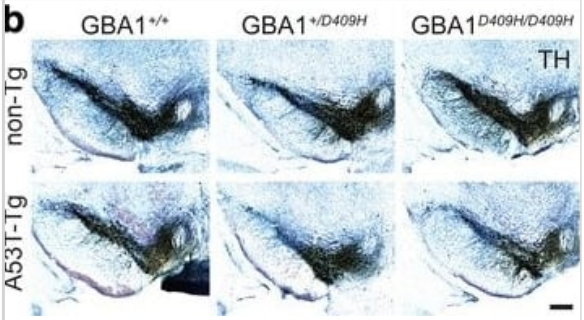

M1 expression pattern changed in trabecular bone. Immunohistochemical staining was performed in sagittal serial sections of medial condyles from 6-week-old rats within the epiphyseal region. The region with the solid line indicates areas of interest to be enlarged in the following image. Representative staining with the anticluster of differentiation 68 (CD68) antibody demonstrated that CD68+ cells were either attached (black arrows) or unattached (white arrows) to the bone surfaces with a variety of sizes and shapes (a, b). TRAP+ cells showed multinucleated morphology (black arrows) which is similar to the CD68+ cells (c, d). Inducible nitric oxide synthase-positive (iNOS+) and C-C chemokine receptor type 7-positive (CCR7+) cells (black arrow) were attached to the bone surfaces with an elongated morphology (e, f, i, j). Arginase1+ and cluster of differentiation 163-positive (CD163+) cells (white arrow) represented the predominant population in the reticular connective tissue with similar expression patterns as in the cortical bone (g, h, k, l). No positive staining was found in isotype controls (data not shown). Most of the M1-labeled cells were found attached to bone surfaces instead of M2-labeled cells (m). Representative images from three independent experiments are shown. FOV, field of view. Data shown as the mean±s.d. (*P<0.05). Image collected and cropped by CiteAb from the following open publication (https://pubmed.ncbi.nlm.nih.gov/29263936), licensed under a CC-BY license. Not internally tested by Novus Biologicals.

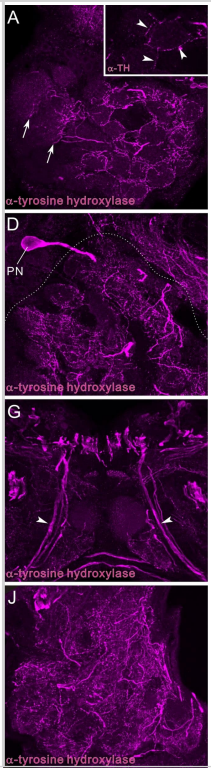

Ubiquitination and autophagy activity can be induced by Mm infection.(A) Schematic diagram of the zebrafish Mm infection model for early stages of Tb. Fluorescently labelled Mm bacteria are microinjected into the blood island of embryos at 28 hpf. Red dots represent small clusters of Mm-infected cells visible from 1 dpi. At 3 dpi these Mm clusters have grown into early stage granulomas. (B) Representative confocal micrographs of GFP-Lc3 co-localization with mCherry-labeled Mm clusters in infected embryos/larvae at 1, 2 and 3 dpi. Scale bars, 10 μm. (C) Quantification of the percentage of Mm clusters positive for GFP-Lc3 at 1 and 2 dpi. The results were accumulated from two individual experiments (≥ 20 embryos/group). ns, non-significant, *p<0.05, **p<0.01, ***p<0.001. (D) Representative confocal micrographs of GFP-Lc3 co-localization with mCrimson-labeled Mm clusters in an mpeg1:mCherry-expressing macrophage at 3 dpi. Arrowheads indicate intra-macrophage GFP-Lc3-positive Mm. Scale bars, 10 μm. (E) Western blot determination of Lc3 protein levels in Mm-infected embryos/larvae and uninfected controls. Protein samples were extracted at 1, 2 and 3 dpi (>10 larvae/sample). The Western blot was probed with antibodies against Lc3 and Actin as a loading control and is representative for three independent experimental repeats. The Lc3-II/Lc3-I ratio is indicated below. (F) Representative confocal micrographs of Ubiquitin antibody co-localization with Mm clusters in infected embryos/larvae at 1, 2 and 3 dpi. Scale bars, 10 μm. (G) Quantification of the percentage of Mm clusters positive for ubiquitin staining at 1 and 2 dpi (≥ 15 embryo/group). The results are accumulated from two independent experiments. ns, non-significant, *p<0.05, **p<0.01, ***p<0.001. (H) Western blot analysis of ubiquitination levels in Mm-infected embryos/larvae and uninfected controls. Protein samples were extracted at 1, 2 and 3 dpi (>10 larvae/sample). The Western blot was probed with an antibody detecting both poly- and mono-ubiquitin and with anti-Actin antibody as a loading control and is representative for three independent experimental repeats. (I) Representative confocal micrographs of GFP-Lc3 and Ubiquitin co-localization with Mm clusters in infected larvae at 3 dpi. Scale bars, 10 μm. Image collected and cropped by CiteAb from the following open publication (https://pubmed.ncbi.nlm.nih.gov/30818338), licensed under a CC-BY license. Not internally tested by Novus Biologicals.

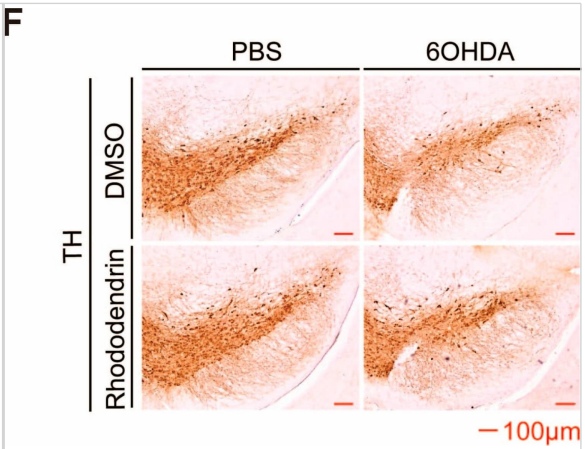

Publications

Grembecka B, Majkutewicz I, Harackiewicz O, Wrona D Deep-Brain Subthalamic Nucleus Stimulation Enhances Food-Related Motivation by Influencing Neuroinflammation and Anxiety Levels in a Rat Model of Early-Stage Parkinsons Disease International Journal of Molecular Sciences 2023-11-29 [PMID: 38069238] (IHC, Rat)

Details:
Dilution 1:1500

Zheng X, Liu Z, He Z et al. Preclinical Long-Term Safety of Intraspinal Transplantation of Human Dorsal Spinal GABA Neural Progenitor Cells iScience 2023-10-01 [PMID: 38026209]

Cara-Esteban M, Marín MP, Martínez-Alonso E et al. The Golgi complex of dopaminergic enteric neurons is fragmented in a hemiparkinsonian rat model Microscopy research and technique 2023-10-19 [PMID: 37855309] (IF/ICC, Rat)

Otani Y, Yoshikawa S, Nagao K et al. Connective tissue mast cells store and release noradrenaline The journal of physiological sciences : JPS 2023-10-12 [PMID: 37828465] (WB, Mouse)

Mao R, Yu J, Deng B et al. Conditional Chemoconnectomics: A Set of Libraries Targeting All Chemical Transmission Corresponding Genes Efficiently bioRxiv 2023-09-28 (IHC, Insect)

Details:
Dilution 1:1000

Puelles L, Stühmer T, Rubenstein JLR, Diaz C Critical test of the assumption that the hypothalamic entopeduncular nucleus of rodents is homologous with the primate internal pallidum The Journal of comparative neurology 2023-11-01 [PMID: 37695031] (IHC, Mouse)

Suzuki T, Hattori S, Mizukami H et al. Inversed Effects of Nav1.2 Deficiency at Medial Prefrontal Cortex and Ventral Tegmental Area for Prepulse Inhibition in Acoustic Startle Response Molecular neurobiology 2023-08-31 [PMID: 37650965]

Marcinkiewcz C, Wang R, Khan K et al. Alcohol inhibits sociability via serotonin inputs to the nucleus accumbens Research Square 2023-08-18 [PMID: 37461716]

Kang JY, Kim DY, Lee JS et al. Korean Red Ginseng Ameliorates Fatigue via Modulation of 5-HT and Corticosterone in a Sleep-Deprived Mouse Model Nutrients 2021-09-06 [PMID: 34578998] (ICC/IF)

Kim H, Huh YJ, Kim JH et al. Identification and evaluation of midbrain specific longevity-related genes in exceptionally long-lived but healthy mice Frontiers in Aging Neuroscience 2023-01-11 [PMID: 36711211] (IHC, WB)

Chen X, Tsika E, Levine N, Moore DJ. VPS35 and ?-Synuclein fail to interact to modulate neurodegeneration in rodent models of Parkinson's disease Molecular Neurodegeneration 2023-08-04 [PMID: 37542299] (WB)

Ryu TH, Subramanian M, Yeom E, Yu K. The prominin-like Gene Expressed in a Subset of Dopaminergic Neurons Regulates Locomotion in Drosophila Molecules and Cells 2022-09-30 [PMID: 35993164] (IHC)

More publications at http://www.novusbio.com/NB300-109

Novus Biologicals USA
10730 E. Briarwood Avenue
Centennial, CO 80112
USA
Phone: 303.730.1950
Toll Free: 1.888.506.6887
Fax: 303.730.1966
nb-customerservice@bio-techne.com

Bio-Techne Canada
21 Canmotor Ave
Toronto, ON M8Z 4E6
Canada
Phone: 905.827.6400
Toll Free: 855.668.8722
Fax: 905.827.6402
canada.inquires@bio-techne.com

Bio-Techne Ltd
19 Barton Lane
Abingdon Science Park
Abingdon, OX14 3NB, United Kingdom
Phone: (44) (0) 1235 529449
Free Phone: 0800 37 34 15
Fax: (44) (0) 1235 533420
info.EMEA@bio-techne.com

General Contact Information
www.novusbio.com
Technical Support: nb-technical@bio-techne.com
Orders: nb-customerservice@bio-techne.com
General: novus@novusbio.com

Products Related to NB300-109

NB820-59217	Human Heart Whole Tissue Lysate (Adult Whole Normal)
HAF008	Goat anti-Rabbit IgG Secondary Antibody [HRP]
NB7160	Goat anti-Rabbit IgG (H+L) Secondary Antibody [HRP]
NBP2-24891	Rabbit IgG Isotype Control

Limitations

This product is for research use only and is not approved for use in humans or in clinical diagnosis. Primary Antibodies are guaranteed for 1 year from date of receipt.

For more information on our 100% guarantee, please visit www.novusbio.com/guarantee

Earn gift cards/discounts by submitting a review: www.novusbio.com/reviews/submit/NB300-109

Earn gift cards/discounts by submitting a publication using this product: www.novusbio.com/publications